N-doped graphitic carbon&Co3O4: The efficient catalyst for degradation of Rhodamine B and 2,4,6-Trichlorophenol in Peroxymonosulfate (PMS) system

HAKKI TÜRKER AKÇAY
Recep Tayyip Erdoğan University: Recep Tayyip Erdogan Universitesi
ADEM DEMİR
Recep Tayyip Erdoğan University: Recep Tayyip Erdogan Universitesi
ZEHRA ÖZÇİFÇİ
Recep Tayyip Erdoğan University: Recep Tayyip Erdogan Universitesi
TUĞRUL YUMAK
Sinop University: Sinop Universitesi
Turgut Keleş (turgut.keles@erdogan.edu.tr)
Recep Tayyip Erdoğan University: Recep Tayyip Erdogan Universitesi https://orcid.org/0000-0002-1911-8020

Research Article

Keywords: cobalt phthalocyanine, peroxymonosulfate, rhodamine B, 2,4,6- Trichlorophenol, catalytic degradation.

Posted Date: March 15th, 2022

DOI: https://doi.org/10.21203/rs.3.rs-1207766/v1

Abstract

One of the most important issues in the world in recent years is water pollution, which is brought about by rapid industrialization. Peroxymonosulfate (PMS) oxidation is an effective technique for wastewater treatment. Transition metals such as cobalt, manganese, iron are used to activate PMS. Therefore, in this study, a novel activated carbon and cobalt phthalocyanine catalyst (Co-AC) was synthesized by the solvothermal method.Rhodamine B (RhB) and 2,4,6-Trichlorophenol (2,4,6-TCP) were used as model pollutants in the catalytic tests. The effective catalytic activity was observed at a low concentration of Co-AC and PMS compared to the literature. XRD, TEM, Raman, SEM and XPS techniques were used for the characterization of the as-synthesized catalyst. In addition, the surface area of Co-AC was calculated by BET and QS-DFT analysis. As a result, the degradation of RhB was found to be 97.07% after 16 minutes, and 100% for 2,4,6-TCP after 6 minutes. Experimental parameters such as temperature, pH, the concentration of the catalyst and PMS were studied and optimum conditions were determined In addition, TOC removal values were found to be 46% for RhB and 66% for 2,4,6-TCP, respectively. The ICP-OES technique was used for the cobalt leaching and the results were found to be 1.35 mgL^{-1} for the RhB solution and 1.38 mgL^{-1} for 2,4,6-TCP. These results are in good agreement with previously published works. The synthesized activated carbon-supported cobalt-based catalyst in line with these results acts as an effective catalyst especially in the treatment of wastewater containing pollutants such as RhB and 2,4,6-TCP.

1. Introduction

Environmental pollution is a threatening problem for the lives of all living beings. Result of the services provided in sectors such as textile, cosmetics, health, agriculture, food industry, many dangerous organic wastes is left to nature. These organic wastes like Rhodamine B (RhB) are widely used in textile, leather, agriculture, food, dyeing while 2,4,6- Trichlorophenol (TCP) is largely employed in producing are fungicides, herbicides, insecticides, and pharmaceuticals industries (Pearce et al. 2003; Ghodbane and Hamdaoui 2009) The release of these pollutants to groundwater is a major problem due to negative effects on human health including cancer, skin and eyes defects, respiratory and cardiovascular disorders. Moreover, it's known that the pollution of water resulting from these pollutants causes a devastating effect threatening to whole life on the ecosystem (Fisher 1973; Roberts et al. 2010). These chemically stable against photo and biological degradation wastes, are removed by different processes including adsorption, filtration, chemical oxidation Fenton-like methods (Wan and Wang 2017; Yazdanbakhsh et al. 2020) electrochemical (Sanromán et al. 2004; Martínez-Huitle and Brillas 2009; Nippatla and Philip 2020) and advanced oxidation processes (AOPs) (Ghanbari et al. 2016; Yuan et al. 2021). Among these methods, AOPs have recently gained interest because of higher degradation yields and shorter process time (Fernandez et al. 2003; Qi et al. 2013; Olmez-Hanci et al. 2015).

AOPs have great attention to the degradation of RhB and 2,4,6-TCP in recent years due to the advantages such as shorter process time, ease of application, higher degradation yield, and low cost (Rasalingam et al. 2015; Ren et al. 2018). Moreover, transition metal-doped catalysts in PMS systems are excellent to

generate radicals. For this purpose, this kind of catalysts/AOPs studies in this field has gradually gained momentum in the last decade years.

Especially, hydroxyl radical and sulfate radical have attracted much attention due to their high redox potential of 2.8 eV and 2.5-3.1 eV, respectively in the presence of peroxymonosulfate (PMS) (Tabit et al. 2018; Wang et al. 2021) and persulfate (PS) (Xie 2017). Sulfate radical ($SO_4^{\cdot -}$) has much promising recently against hydroxyl radical (OH·) because of its high redox potential, applicable wide pH range and long lifetime (Xu et al. 2019). Generally, sulfate radical is produced by peroxydisulfate (PDS) or peroxymonosulfate and activated by heating (Ji et al. 2016), UV-irradiation (Upadhyay et al. 2020), transition metal ions, or metal oxide analogs (Hardjono et al. 2011; Wang et al. 2020b) and carbon-based materials (Gunture et al. 2019; Zuo et al. 2021).

Several works reported that the cobalt-based /PMS catalysis has possessed a great performance in the degradation of organic pollutants (Korzeniowska et al. 2020; Dou et al. 2020; Hou et al. 2021). As reported earlier, transition metal ions like Co(II) can activate PMS to generate sulfate radicals as below (Eqs. (1)-(7)) (Yuan et al. 2011), (Yang et al. 2008; Ling et al. 2010; Antoniou et al. 2010).

$$Co^{2+} + H_2O \longleftrightarrow CoOH^+ + H^+ \quad (1)$$

$$Co^{2+} + HSO_5^- \longrightarrow Co^{3+} + SO_4^{\cdot -} + OH^- \quad (2)$$

$$CoOH^+ + HSO_5^- \longrightarrow CoO^+ + SO_4^{\cdot -} + H_2O \quad (3)$$

$$CoO^+ + 2H^+ \longleftrightarrow Co^{3+} + H_2O \quad (4)$$

$$Co^{2+} + SO_4^{\cdot -} \longrightarrow Co^{3+} + SHO_4^{2-} \quad (5)$$

$$Co^{2+} + \cdot OH \longrightarrow Co^{3+} + OH^- \quad (6)$$

$$Co^{3+} + HSO_5^- \longrightarrow Co^{2+} + SO_5^{\cdot -} + H^+ \quad (7)$$

L. Hu et al. (Hu et al. 2013) synthesized a novel heterogeneous Co catalyst CoMg/SBA-15 resulting in a significant performance with nearly 100% degradation in the presence of PMS in 5 min. Moreover, this catalyst displayed stable reusability up to 25 runs. Y. Li et al. (Li et al. 2020b) designed $CoFe_2O_4$/HPC in graphitized structure to investigate the degradation of bisphenol A and the results showed that this catalyst was found to be the superiority of among other counterparts by indicating 100% degradation of bisphenol A in 8 min and 80% degradation up to 5 runs for reusability. Q. Song et al. (Song et al. 2019) investigated the degradation of triphenyl phosphate by $CoFe_2O_4$ catalyst activated PMS system and found that it is removed by 99.5% after 6 min, and discussed the influence of PMS concentration, initial pH, anion and humic acid on the degradation of triphenyl phosphate. In recent a study, H. Zhang et al. (Zhang et al. 2020) prepared Co doped $ZnFe_2O_4$ nanoparticles to degradate bisphenol A in PMS system and achieved completely 100% degradation in 4 min. This catalyst maintain its stability between pH 3 and pH 11 by demonstrating about 80-90% degradation of bisphenol A. Researchers are still working on

the development of cost and process-effective catalysts to be used in wastewater treatment (Caparrós et al. 2012; Xiao et al. 2020).

Phthalocyanines are planar macrocyclic structures having good thermal stability. Thanks to their thermally stable structures, these compounds keep their basic planar structure even at high temperatures that generally most of the organic compounds are decomposed. The strong π conjugation supplied by delocalized 18-π electrons, besides gaining stability to the structure, gives a graphite-like form (Dignard-Bailey et al. 1994; Li et al. 2018). In addition, nitrogen atoms in the phthalocyanines have unpaired electrons that could attend in electron transfer mechanisms. Therefore, chemically inactive, carbonized forms of phthalocyanine could be a good catalyst for the degradation of most organic chemicals, thanks to their nitrogen contents and graphite-like structures. It would be beneficial to bind the phthalocyanines to a porous support layer to prevent aggregation, which could reduce the effectiveness of the catalyst.

To the best of our knowledge, activated carbon is the most extensively used adsorbent for water treatment. Most types of that have not only high surface area but also have hetero atom containing surface functional groups that affect the surface charge as well (Valdés et al. 2002; Wang et al. 2020a). Their adsorption properties can be altered by modifying their pore structure, pore size distribution and surface chemical properties (Bell et al. 2011). We aimed to create “reaction holes” on the activated carbon surface to decrease the degradation time by increasing the interaction of radical species and the pollutants. Therefore, commercial activated carbon with a high surface area and many accessible pores were used as the support to facilitate the adhesion of molecules of organic pollutants into these “reaction holes”. In line with this hypothesis, the preparation of cobalt phthalocyanine-based carbon catalysts that could be used in wastewater treatment is the essential motivation of this study. For this purpose, Co-AC catalyst was prepared through the phthalocyanine cobalt(II) complex was carbonized with the commercial activated carbon under N_2 atmosphere. The product was characterized by X-Ray Powder Diffraction (XRD), Scanning Electron Microscopy (SEM), Transmission Electron Microscopy (TEM), Raman, and cryogenic N_2 adsorption techniques. RhB and 2,4,6-TCP were chosen as model pollutants for water treatment and the catalytic activity of Co-AC was investigated with different conditions.

2. Experimental

2.1. Material and Methods

RhB ($C_{28}H_{31}ClN_2O_3$) ≥ 95%, 2,4,6-Trichlorophenol (2,4,6-TCP) 98%, Oxone ($2KHSO_5{\cdot}KHSO_4{\cdot}K_2SO_4$)>95%, phthalonitrile (99%), cobalt (II) chloride (97%), ethanol (99.8), tetrahydrofuran (THF) ≥99.9, *tert*-butyl alcohol (TBA) ≥99.5, *p*-Benzoquinone (*p*-BQ) ≥98 and trolox 97% were purchased from Sigma-Aldrich. The commercial activated carbon was purchased by a local supplier, and it was dried for 3 hours at 120°C before use. All stock solutions were prepared with deionized water by using Human Corporation Zeneer Power 1 water purification instrument.

The XRD spectra were recorded in Rigaku smart lab system. The SEM and EDS images of materials were obtained using a JEOL. The TEM images of samples were recorded by Hitachi HT-7700 equipped with the Lanthanum hexaboride electron beam gun with 40-120 eV. Surface area and porosity were studied by BET analyzer (Quantachrome, USA) by nitrogen adsorption at −196°C. The degassed of samples was performed under vacuum at 105°C for fifteen hours before the measurement. The surface area, total pore volume, pore size distribution of AC and Co-AC were calculated by Brunauer–Emmett–Teller (BET) method, the Quenched Solid Density Functional Theory (QS-DFT) and Barrett-Joyner-Halenda (BJH) method (Evans and Tarazona; Kwiatkowski and Broniek 2020).

The catalytic activity of Co-AC was determined under different pH, temperature, catalyst and PMS concentrations by using Thermo Scientific Multiskan Go UV/VIS spectrophotometer at 554 nm for RhB but TCP was measured by Thermo Scientific Fınnıgan HPLC at 280 nm. Also, cobalt leaching was analyzed with ICP-OES OPTİMA 7000 DV (Perkin Elmer). Moreover, reusability of catalyst was studied and radical scavenging experiments were applied in presence of various radical scavengers such as ethanol (EtOH) for $SO_4^{\cdot -}$ and OH·, tert-butanol (TBA) for OH·, *p*-Benzoquinone (*p*-BQ) for $O_2^{\cdot -}$ also Trolox was chosen for non-radical trials.

2.2 Experimental Procedures

2.3 Preparation of Co-AC catalyst

200 mg phthalocyanine (II) complex and 200 mg commercial activated carbon were mixed in 50 mL of THF and stirred for 3 days at room temperature. After that THF was evaporated and the resulting solid was carbonized for one hour at 800°C under 100 mL min^{-1} N2 flowing then washed with water three times.

2.4 Catalytic performance of Co-AC

To investigate the catalytic performance of Co-AC, the degradation of RhB via PMS was chosen as a model catalytic reaction. The decrease of absorption peak (λ_{max} = 554 nm) of RhB was monitored with Thermo Scientific Multiskan Go UV/Vis spectrophotometer at 25 ^{o}C. While no significant change in the absorption peak of RhB without Co-AC, at end of 30 min of adsorption-desorption time 15% reductions of maximum absorption peak in the catalyst system without PMS were observed. The degradation of RhB was measured 97.07% in 16 min in the experimental system consisting of 12 mgL^{-1} RhB aqueous solution, Co-AC, and PMS (150 mgL^{-1} and 90 mgL^{-1}, respectively) in Fig. 7. After a certain period of reaction, sample solutions were filtered via syringe with a filter (0.45 µm) and analyzed at 554 nm. For 2,4,6-TCP, the same operations were applied by using 150 mgL^{-1} of Co-AC catalyst and 25 mgL^{-1} the aqueous solution of 2,4,6-TCP and 100% degradation was obtained at the end of 6 min in Fig. 8. The reaction was monitored by HPLC at 280 nm. Under the same steps, the effects of different reaction temperatures, pH values, amounts of PMS, and Co-AC on the catalytic reaction were examined. According

to the results, the kinetic parameters of catalytic degradation of RhB and 2,4,6-TCP followed the pseudo-first-order model Eqs 8.

$$\ln (C/C_0) = -kt \quad (8)$$

Where, "C_0" is the initial concentration of RhB and 2,4,6-TCP, "C" is the concentration of at the time "t", "k" is the first-order reaction rate constant. The kinetic parameters were calculated as the literature (Sundar et al. 2008). Thus, the degradation of RhB and 2,4,6-TCP in presence of Co-AC/PMS was studied in the following experiments.

2.5 Degradation of RhB and 2,4,6-TCP and other catalytic parameter experiments

The catalytic activity of Co-AC was investigated with degradation of RhB in deionized aqueous solutions and the degradation experiments were applied in a 100 mL glass bottle with magnetic stirring at 25 ^{o}C. Firstly, the solution of RhB (12 mgL^{-1}) was prepared with deionized water and the initial concentration of Co-AC catalyst was determined as 7.5 mg. The 100 mL of dye solution and 7.5 mg catalyst were vigorously stirred at 25 ^{o}C to form an adsorption-desorption equilibrium between Co-AC and RhB and then the degradation reaction was started with 9 mg PMS was added to the reaction mixture. The course of the degradation reaction was monitored by measuring their absorbance at 554 nm that periodically sampled and filtered aliquots from the main solution. To stop the degradation reaction, the catalyst was removed from aliquots by filtering with 0.45 µm PTFE syringe filter. The absorbance values were recorded by Thermo Scientific Multiskan Go UV/Vis spectrophotometer. The degradation experiments of 2,4,6-TCP were applied similarly to that of RhB. 25 mgL^{-1} 2,4,6-TCP stock solution was prepared and used in 100 mL portions. The 100 mL 2,4,6-TCP solution and 10 mg Co-AC catalyst were incubated by stirring at 25 ^{o}C to set adsorption-desorption equilibrium. After, 6 mg PMS was added in reaction media to start the reaction. The course of the degradation reaction was monitored as in sampling of degradation of RhB by HPLC at 280 nm. (The concentration of TCP was measured by HPLC with C18 column (250 mm × 4.6 nm, 5µm) and diode-array-detector, mobile phase consisted acetonitrile/water (60:40 volume ratio), 0.1% formic acid and the column flow rate was gone through with 0.6 mL min^{-1}) (Rasalingam et al. 2015). Moreover, the effects of the catalyst concentration (50 to 150 mgL^{-1}), PMS concentration (30 to 120 mgL^{-1}), pH (2-11) and temperature of the solution (25 ^{o}C, 35 ^{o}C and 45 ^{o}C) were studied on the catalytic activity of RhB. Similarly for TCP, PMS concentration was determined in the range of 50 to 150 mgL^{-1} for catalyst and 30 to 120 mgL^{-1} for PMS, the range of pH value 2 to 11 and temperature (25 ^{o}C, 35 ^{o}C and 45 ^{o}C) to obtain optimum catalyst efficiency. The reusability experiments of RhB and 2,4,6-TCP were performed by the addition of fresh RhB and 2,4,6-TCP solutions at the end of the first cycle and the same procedure was performed for other cyles. In the radical scavenging experiments, to distinguish active radical species such as $SO_4^{\cdot -}$, OH·, $O_2^{\cdot -}$ and $^1O_2$. The ethanol (EtOH), *tert*-butyl alcohol (TBA), and *p*-Benzoquinone (*p*-BQ) were used for quenching $SO_4^{\cdot -}$ or OH·, OH· and $O_2^{\cdot -}$respectively as a radical

quencher (Bisbyb et al. 1999). In addition, Trolox was used for $^1O_2$ quencher (Khan et al. 2018) according to determined concentrations in the Co-AC/PMS system.

3. Results And Discussion

3.1. Characterization of Co-AC catalyst

Figure 1 shows the XRD pattern of the Co-AC. The peaks at 2θ 18.96, 31.32, 36.8, 44.28, 59.50, 65.34° corresponding to (111), (220), (311), (400), (511) and (440) respectively, which are consistent with the standard card JCPDS No. 42-1467 with the lattice constant a = 0.8084 nm (space group Fd-3m [227]). Also, the peak observed at 2θ 26.08°, 42.44°, are assigned as graphite-like structures (Kamar and Sheha 2017; Klepel et al. 2021; Jiang et al. 2021). The clear XRD pattern of Co-AC shows that there are no impurities in the product.

The N_2 adsorption-desorption isotherms of AC and Co-AC in Fig. 2 are assigned as type-II with H4 type hysteresis, which was with slit shape, commonly observed in activated carbon materials (Üner and Bayrak 2018; Lu et al. 2021). As can be seen in Table 1, the addition of phthalocyanines cobalt (II) decreases the specific surface area of AC from 904.1 to 256.2 m^2g^{-1}. This is evidence that the phthalocyanine cobalt (II) complex adsorbed -into micro and mesoporous of AC as expected. It's probably, during the furnaced, phthalocyanines ring fused with functional sites on activated carbon.

Table 1
Specific surface properties of AC and Co-AC

	BET	**BJH**	**QS-DFT**	
Sample	Surface Area m^2g^{-1}	Surface Area m^2g^{-1}	Pore volume mLg^{-1}	Surface Area m^2g^{-1}
AC	904.1	208.8	0.64	1042.4
Co-AC	256.2	114.8	0.215	279.1

The specific surface area of AC and Co-AC catalysts were calculated by BET and QS-DFT methods and were determined as 904.1 and 256.2 m^2g^{-1} for BET; 1042.4 and 279.1 m^2g^{-1} for QS-DFT, respectively (Kumar and Jena 2016). According to the BJH method, the specific surface area of AC and Co-AC was found to be 208.8 and 114.8 m^2g^{-1} respectively. This situation showed that both AC and Co-AC consisted of both micropores and mesopores. The pore size distribution of the AC and Co-AC calculated by the QS-DFT method in Fig. 3 was consistent with BJH and QS-DFT values. The total pore volume of AC and Co-AC were calculated as 0.64 and 0.215 mLg^{-1} by the QS-DFT method.

The SEM images and EDS analysis show that Co-AC has channeled 3D porous structure and the structure contains carbon, nitrogen, oxygen, and cobalt elements as homogenously distributed throughout the Co-

AC in Fig. 4. The cobalt and oxygen content of 9.6% and 26% respectively show that the carbonized structure probably contains carbonyl oxygen except for oxygen of Co_3O_4. In addition, the presence of nitrogen element signs that nitrogen atoms successfully were doped on the Co-AC. The TEM images (Fig. 5) illustrate the nano-dot morphology of Co-AC. The dots with contrast show the presence of Co_3O_4 and carbon structure (Aluha et al.). As can be seen in Fig. 5 (a) and (d) the carbonized structure consists of graphitic layered forms confirmed by carbon peaks of XRD and Raman spectra.

The graphitization degree of AC and Co-AC samples were investigated by Raman spectroscopy. As can be seen in Fig. 6, the bands caused by graphite (G) and defect-disorder (D) were observed at about 1580 cm^{-1} and 1350 cm^{-1}, respectively. The ratio of integrated intensities of these bands (I_D/I_G) is a measure of graphitization and crystallinity of carbonaceous material. As a rule, while I_D/I_G ratio increases, crystallinity decreases and graphitization increases (TUINSTRA F and KOENIG JL 1970; Le Van and Luong Thi Thu 2019). The I_D/I_G values of AC and Co-AC samples were calculated as 1.12 and 1.21. The increasing I_D/I_G value of Co-AC clearly shows that the doping of phthalocyanine cobalt complex on activated carbon caused to increase in the surface disorder degree. The increase of the surface disorder degree is due to partial degradation of the planar structure of phthalocyanines. Especially isoindole moiety of phthalocyanine could be the main source of this disorder. While the planar form of phthalocyanine ring supports the graphitization during the heating treatment, the degradation in the center of the phthalocyanine ring starting with the transformation of Co^{2+} to Co_3O_4 could cause increasing in defect-disorder. Table 2 illustrates the comparison of the catalytic activity of Co-AC catalyst in RhB and 2,4,6-TCP solutions with previously reported different catalysts. It could be seen that Co-AC provides a high reaction yield and short reaction time compared to other catalysts for both degradations of RhB and 2,4,6-TCP.

Table 2
Degradation of RhB and 2,4,6-TCP with including different transition metal-based-catalysts in PMS system.

Catalysts	Substrate	Reaction Condition	Reaction Time	References
$CoFe_2O_4$/GO	RhB	0,03 mM RhB, 0.1 mgL^{-1} PMS, 10 mg catalyst, T= 25 ^oC	98% for 12 min	(Tabit et al. 2018)
3%$FeCo_2O_4$/CN	RhB	20 mgL^{-1} RhB, 0.15 gL^{-1} PMS, 0.1 gL^{-1} catalyst and T= 25 ^oC	98% for 45 min	(Zhao et al. 2021)
S-CuMnO	2,4,6-TCP	20 mgL^{-1} TCP, 0.8 mM PMS, 0.07 gL^{-1} catalyst, pH = 7 and T= 25 ^oC	100% for 30 min	(Rasalingam et al. 2015)
CoAl-CLDH-300	RhB	10 mgL^{-1} RhB, 0.15 gL^{-1} catalyst, 0.5 mM PMS, T= 25 ^oC, pH= 5	99.6% for 30 min	(Zhu et al. 2019)
α-MnO_2	RhB	20 mgL^{-1} RhB, 0.1 gL^{-1} catalyst and 0.2 gL^{-1} PMS	99% for 60 min	(Liu et al. 2016)
FePTS	2,4,6-TCP	0.1 mmol TCP solution, 5 $\times 10^{-4}$ mmol catalyst and 0.1 mmol PMS in 0.5 ml aqueous solution	74% for 30 min	(Günay and Çimen 2017)
C@Cu-Ni	2,4,6-TCP	10 mgL^{-1} TCP, 0.1 gL^{-1} catalyst, 1 mM PMS, pH= 5	98.5% for 30 min	(Zhang et al. 2021)
AC	2,4,6-TCP	50 mgL^{-1} TCP, 0.75 gL^{-1} AC, 8 mM PMS, pH= 5	67.3% for 150 min	(Ghanbari et al. 2016)
Co-AC	RhB	12 mgL^{-1} RhB, 150 mgL^{-1} catalyst, 90 mgL^{-1} PMS, T= 25 ^oC	97.07% for 16 min	This work
	2,4,6-TCP	25 mgL^{-1} TCP, 150 mgL^{-1} catalyst, 90 mgL^{-1} PMS, T= 25 ^oC	100% for 6 min	This work

4. Effect Of Reaction Parameters On The Degradation Of Rhb And 2,4,6-tcp

4.1. Effect of catalyst concentration

The effect of the concentration of Co-AC on catalytic performance was studied for catalytic degradation of RhB. The increase of catalyst concentration displayed a positive effect on catalytic degradation experiments in Fig. 9 (A). According to results, about 75% degradation was achieved with 100 mL (12 mgL^{-1}) RhB dye solution, 75 mgL^{-1} catalyst and 90 mgL^{-1} PMS at 25 ^oC at the end of the 16 min (k=

0,0868 min^{-1}). After, the maximum degradation of RhB has observed the maximum catalyst concentration as 150 mgL^{-1} (97.07% degradation, 16 min, k= 0,2206 min^{-1}). For 2,4,6-TCP, the increasing concentration of Co-AC displayed a positive effect on catalytic activity in degradation experiments. For instance, 94% degradation was obtained by using 5 mg Co-AC catalyst, 9 mg PMS and 25 mgL^{-1} 2,4,6-TCP 100 mL solution, after 38 min (k= 0.0740 min^{-1}). By increasing catalyst concentration to 15 mg, 100% degradation was achieved at the end of 6 min in Fig. 10 (A).

As expected when catalyst concentration was increased, more the greater number of active sites interacted with to activate PMS. The increased activated sites could accelerate reaction to generate more radicals for degradation efficiency of RhB and 2,4,6-TCP.

4.2. Effect of PMS concentration

The radicals have an important role due to their high oxidation potentials for the degradation of pollutants. PMS is an important reagent due to take the role of the production of radicals such as $SO4^{\cdot -}$ and OH· in the advanced oxidation process. This oxidant is activated by the catalyst and generates the radicals. Therefore, in addition to the type and concentration of catalysts, the concentration of PMS is highly important too and has a decisive effect on the course of the degradation reaction. It could be expected that the how much radicals form in the solution, the more degradation in presence of enough pollutants. But the low catalyst concentration limits the generation of the radicals. In this regard, the effect of increasing concentration of PMS on the degradation of RhB and 2,4,6-TCP was shown in Fig. 9 (B) and 10 (B). PMS concentration was selected from 1,5 mg (0,024 mM) to 12 mg (0,196 mM) for RhB. The results showed that the maximum degradation was achieved by 6 mg PMS concentration (k= 0,1676 min^{-1}) at the end of 16 min. When PMS concentration was increased to 12 mg, degradation reduced about 9% at the end of the 16th min (k= 0,1125 min^{-1}). This reduction can be due to high PMS concentration acting as a scavenger for sulfate radical (Ghanbari and Moradi 2017). According to these results, the maximum amount of the radical production is limited by fixed catalyst concentration. While at the low concentration of PMS, color removal efficiency and rate constant significantly diminished but at the highest concentration of PMS, catalytic activity slightly decreased.

4.3. Effect of temperature on degradation of RhB

To investigate the effect of temperature on the degradation of RhB and 2,4,6-TCP, the reactions were implemented at different temperatures as shown in Fig. 9 (C) and 10 (C). It was observed that almost all of RhB was degraded when the temperature increased from 25 ^{o}C to 45^{o}C, in a much shorter time than that of reactions at the lower temperature, when the other conditions held constant (Co-AC (75 mgL^{-1})/PMS (90 mgL^{-1})). Compared the degradations at 25 ^{o}C, 35 ^{o}C, 45 ^{o}C temperatures in 10 min, 75.07% (k= 0,0868 min^{-1}), 86.77% (k= 0,1264 min^{-1}) and 97.38% (k= 0,2276 min^{-1}) yields were obtained, respectively.

For 2,4,6-TCP, the temperature was increased from 25$^{\circ}C$ to 45$^{\circ}C$ and catalytic degradation accelerated and 100% degradation was obtained at 45°C. With temperature rising, k= 0.0891 min^{-1} for 25°C, k= 0.1941

min^{-1} for 35°C, k= 0.9780 min^{-1} for 45°C reaction rate constants were achieved in 4 min. The results showed that catalytic activity increased with raising the temperature for both the contaminants.

4.4. Effect of pH

The effect of initial pH values of RhB and 2,4,6-TCP aqueous solutions on degradation efficiency were investigated from 2 to 11 for RhB and 2,4,6-TCP throughout a 16 min period of the reaction time in Fig. 9 (D) and 10 (D). Comparision of the acidic and basic conditions, it was seen the catalyst was more suitable and efficient at pH values 5 and 9 for catalytic degradation of RhB. When pH value was increased from 9 to 11 or decreased from 5 to 2 degradation efficiency decreased from 96.4 to 4.4% or from 93.2–13.22%. The obtained results showed that this decline in degradation may result in PMS due to self-decomposed with a non-radical route (Wang and Chu 2011) due to H^+ ions can quench $SO_4^{\cdot -}$ and OH· radicals at very low pH 2 values as below Eqs (9), (10). Moreover, the form of PMS in the current solution is defined by dye solution pH such as HSO_5^- is the main species in acidic and neutral pH values (Huang et al. 2009; Di et al. 2020).

When the effect of pH on degradation of 2,4,6-TCP was examined, catalyst worked effectively in the range of pH 5 and 9 with 86% (k= 0.1966 min^{-1}), 91% (k= 0.2407 min^{-1}) yields for 10 min. The degradation yield diminished to 54% and 17% at pH 3 and 11 respectively. These decreases in degradation occurred due to mentioned above reasons.

$$\cdot OH + H^+ + e^- \longrightarrow H_2O \quad (9)$$

$$SO_4^{\cdot -} + H^+ + e^- \longrightarrow HSO_4^{\cdot -} \quad (10)$$

5. Radical And Non-radical Quenching Experiments

In general, activated PMS by transition metal oxides could produce $SO_4^{\cdot -}$, OH· and $SO_5^{\cdot -}$radicals (Anipsitakis et al. 2005). $SO_4^{\cdot -}$ and OH· radicals are major active species between these radicals for catalytic degradation of organic pollutants. Ethanol (EtOH) is usually used as a scavenger for quenching $SO_4^{\cdot -}$ and OH· radicals due to their high reaction rate constants k= 1.2×10^9 - 2.8×10^9 $M^{-1}s^{-1}$ for OH· and 1.6×10^7 - 7.7×10^7 $M^{-1}s^{-1}$ for $SO_4^{\cdot -}$ (Yang et al. 2015). Besides, *tert*-butyl alcohol (TBA) is chosen only as scavenger OH·radicals because its reaction rate constant for OH· (k= 3.8×10^8 - 7.6×10^8 $M^{-1}s^{-1}$) is significantly higher than that for $SO_4^{\cdot -}$ (k= 4×10^5 - 9.1×10^5 $M^{-1}s^{-1}$) (Yang et al. 2015). In this regard, we studied with 50 mM TBA and EtOH, scavenger/PMS (5000:1) ratio, as a scavenger to determine major reactive radical species in the Co-AC/PMS system for quenching experiments. As shown in Fig. 11 (A), catalytic degradation of RhB without any EtOH and TBA as no scavenger was 93.18% (k= 0.1678 min^{-1}) for 16 min. However, catalytic degradation was decreased from 93.18–87% and 83.7% in presence of TBA and EtOH, respectively. The reaction rate constants were obtained 0.1132 min^{-1} for EtOH and 0.1275 min^{-1} for TBA. As compared to catalytic degradation efficiency with EtOH and TBA, the further

degradation in the presence of TBA was seen and $SO_4^{\cdot -}$ radical was dominant than OH· radical in the Co-AC/PMS system. In addition, we observed degradation of RhB significantly reduced with addition to *p*-BQ as $O_2^{\cdot -}$ quencher (k= 0,0205 min^{-1}) and Trolox as $^1O_2$ quencher (k= 0.0094 min^{-1}). According to these reaction rate constants, $^1O_2$ radical was superior to other radical species in the quenching experiments.

For 2,4,6-TCP, radical quenching experiments were applied with a similar procedure of RhB as shown in Fig. 11 (C). The reaction rate constant values were 0.1078 min^{-1} for EtOH, 0,1660 min^{-1} for TBA, 0.0843 min^{-1} for *p*-BQ and 0.0287 min^{-1} for Trolox. In line with the obtained results, degradation of 2,4,6-TCP decreased from 86–25% with the addition of Trolox. In this way, $^1O_2$ radical was more effective than other radicals for degradation. The Co-Ac/PMS system displayed both radical ($SO_4^{\cdot -}$, OH·, $O_2^{\cdot -}$) and non-radical ($^1O_2$) pathways according to obtained experimental data.

6. The Stability And Reusability Of Co-ac Catalyst

The stability of Co-AC catalyst (100 mgL^{-1}) was investigated with a reusability experiment of the degradation of RhB (12 mgL^{-1}) in the presence of PMS (90 mgL^{-1}) as shown in Fig. 11 (B). When each cycle ended, a fresh concentrated solution of RhB to obtain the initial concentration of RhB and 6 mg PMS were added to the reaction media. Five cycles were studied for stability and 96.03% degradation was seen at the end of the first cycle for 16 min. After, 93.11, 91.06, 89.49, 88.5% degradation efficiency was obtained at the end of five cycles, respectively. As a result of this study, Co-Ac catalyst exhibited good stability and efficiency with 88.5% degradation at end of the 5 cycles for 62 min.

For the stability and reusability Co-AC in 25 mgL^{-1} of 2,4,6-TCP solution, 100 mgL^{-1} catalysts and 60 mgL^{-1} PMS were chosen for the first cycle and obtained 98.3% degradation for 20 min. Then, for the other cycle, the fresh concentrated 2,4,6-TCP solution was poured into reaction media and 6 mg PMS was added like the above procedure of RhB. At the end of the five cycles, 87% degradation was achieved for 60 min as shown in Fig. 11 (D). This Co-AC catalyst displayed nearly the same stability and efficiency for both RhB and 2,4,6-TCP contaminants.

7. Toc And Icp-oes Analysis

To investigate the mineralization degree of RhB and 2,4,6-TCP, Total organic carbon (TOC) removal efficiency of Co-AC/PMS was tested in the catalytic oxidation process. TOC analysis was performed by Shimadzu TOC-L analyzer. It is clear from the obtained results that TOC removal % was 46 for RhB while it was 66 for 2,4,6-TCP at the end of the reactions in Fig. 12. Compared to TOC removal value of RhB with that of 2,4,6-TCP, The lower TOC removal may be due to resistance of the aromatic RhB oxidation products (Huang and Huang 2009).

Transition metal leaching is an important issue in heterogeneous catalyst systems as it has a potential threat to the environment. Moreover, cobalt is known as a superior activator for PMS and high cobalt leaching shows a negative effect on the degradation of organic wastes as catalyst performance decreases (Pang et al. 2020). Therefore, the cobalt leaching tests were separately performed for RhB and 2,4,6-TCP. The solutions obtained at the end of the reactions were diluted to certain amounts and analyzed with ICP-OES OPTİMA 7000 DV (Perkin Elmer). According to the results, the leaching values of cobalt were 1.35 mgL^{-1} and 1.38 mgL^{-1} for RHB and 2,4,6-TCP, respectively as shown in Fig. 12. Our study is acceptable when these values were compared to previous works such as 1.669 mgL^{-1} for $MnCo_2O_{4.5}$ (Dung et al. 2020), 9 mgL^{-1} for Co-BTC(A) (Li et al. 2016), 63.18 mgL^{-1} for activated carbon(AC) supported Co_3O_4 based catalyst (Erdem and Erdem 2020), 1.82 mgL^{-1} for Co-SMA (Mahamallik and Pal 2020), 1 mgL^{-1} for BC- Co_3O_4 (Chen et al. 2018), 0.9 mgL^{-1} for $CoFeO_2$@CN and 1.4 mgL^{-1} for pristine $CoFeO_2$ (Pi et al. 2020), 3.23 mgL^{-1} for commercial Co_3O_4 (Kang and Hwang 2021), 3 mgL^{-1} for Co_1Fe_1-300 (Li et al. 2020a), in the literature.

Conclusion

In this study, phthalocyanine Co(II) complex was impregnated in commercial activated carbon and the product was carbonized at 800°C. N_2 adsorption studies showed that phthalocyanine Co(II) was located to microporous smaller than 2 nm. It was confirmed by analysis of SEM, XRD, TEM and Raman that Co-AC also consists of graphite-like layered structures and contains nitrogen atoms. The catalytic degradation system was set on Co-AC, PMS and model organic pollutants. The catalytic efficiency of Co-AC on organic pollutants was investigated by model compounds RhB 2,4,6-TCP. Within the scope of the catalytic study, the effect of PMS concentration, reaction temperature, the concentration of catalyst, the pH of the solution on the reaction rate and recycling performance was investigated and optimal conditions were determined. 97% degradation value was observed in 16 min at 25°C but no pH adjustment. In addition, 97.38% degradation was reached by increasing temperature up to 45°C in 10 min and optimum pH value was obtained at 9 but degradation decreased to 4.4% at pH 11. At the end of five cycles, 88.5% stability was observed in RhB/PMS system. For 2,4,6-TCP, 100% degradation was seen in 6 min at 45°C without applying pH. The degradation efficiency was diminished to 17% by high pH. If we compare the catalyst efficiency for RhB and 2,4,6-TCP, it is found that Co-AC is more effective in a shorter time for 2,4,6-TCP. Comparing our results with the previously reported, it can be said that the Co-AC may be the model catalyst for both degradations of RhB and 2,4,6-TCP. In further studies, the catalytic activity of Co-AC could be tested other organic pollutants/PMS systems thanks to its high reaction yield, short reaction time, and moderate recycling performance.

Declarations

Ethical Approval

Not applicable

Consent to Participate

Not applicable

Consent to Publish

Not applicable

Authors Contributions

All authors contributed to the study's conception and design. Material preparation, data collection and analysis were performed by Hakkı Türker Akçay, Adem Demir, Zehra Özçifçi, Tuğrul Yumak and Turgut Keleş. The first draft of the manuscript was written by Turgut Keleş and all authors commented on previous versions of the manuscript. All authors read and approved the final manuscript.

Conceptualization: [Turgut KELEŞ], [Hakkı Türker AKÇAY]; Methodology: [Hakkı Türker AKÇAY]; Formal analysis and investigation: [Turgut KELEŞ], [Adem DEMİR], [Zehra ÖZÇİFÇİ], [Tuğrul YUMAK]; Writing - original draft preparation: [Turgut KELEŞ]; Writing - review and editing: [Hakkı Türker AKÇAY], [Tuğrul YUMAK]; Supervision: [Turgut KELEŞ].

Funding

The authors declare that no funds, grants, or other support were received during the preparation of this manuscript.

Competing Interests

The authors declare that they have no known competing financial interests or personal relationships that could have appeared to influence the work reported in this paper.

Availability of data and materials

Not applicable

References

1. Aluha J, Abatzoglou N, Gitzhofer F Production of active carbon-supported Fischer-Tropsch nano-catalysts using induction suspension plasma-spray (SPS) technology
2. Anipsitakis GP, Stathatos E, Dionysiou DD (2005) Heterogeneous activation of Oxone using Co 3O 4. J Phys Chem B 109:13052–13055. https://doi.org/10.1021/jp052166y
3. Antoniou MG, de la Cruz AA, Dionysiou DD (2010) Degradation of microcystin-LR using sulfate radicals generated through photolysis, thermolysis and e- transfer mechanisms. Appl Catal B Environ 96:290–298. https://doi.org/10.1016/j.apcatb.2010.02.013

4. Bell JG, Zhao X, Uygur Y, Thomas KM (2011) Adsorption of chloroaromatic models for dioxins on porous carbons: The influence of adsorbate structure and surface functional groups on surface interactions and adsorption kinetics. J Phys Chem C 115:2776–2789. https://doi.org/10.1021/jp1099893
5. Bisbyb RH, Morgan CG, Hamblett I, Gorman AA (1999) Quenching of Singlet Oxygen by Trolox C, Ascorbate, and Amino Acids: Effects of pH and Temperature. J Phys Chem A 103:7454–7459. https://doi.org/10.1021/jp990838c
6. Caparrós C, Benelmekki M, Martins PM, et al (2012) Hydrothermal assisted synthesis of iron oxide-based magnetic silica spheres and their performance in magnetophoretic water purification. Mater Chem Phys 135:510–517. https://doi.org/10.1016/j.matchemphys.2012.05.016
7. Chen L, Yang S, Zuo X, et al (2018) Biochar modification significantly promotes the activity of Co3O4 towards heterogeneous activation of peroxymonosulfate. Chem Eng J 354:856–865. https://doi.org/10.1016/j.cej.2018.08.098
8. Di J, Zhu M, Jamakanga R, et al (2020) Electrochemical activation combined with advanced oxidation on NiCo2O4 nanoarray electrode for decomposition of Rhodamine B. J Water Process Eng 37:. https://doi.org/10.1016/j.jwpe.2020.101386
9. Dignard-Bailey L, Tradeau ML, My A, et al (1994) Graphitization and particle size analysis of pyrolyzed cobalt phthalocyanine/carbon catalysts for oxygen reduction in fuel cells
10. Dou R, Cheng H, Ma J, Komarneni S (2020) Manganese doped magnetic cobalt ferrite nanoparticles for dye degradation via a novel heterogeneous chemical catalysis. Mater Chem Phys 240:. https://doi.org/10.1016/j.matchemphys.2019.122181
11. Dung NT, Thu TV, Van Nguyen T, et al (2020) Catalytic activation of peroxymonosulfate with manganese cobaltite nanoparticles for the degradation of organic dyes. RSC Adv 10:3775–3788. https://doi.org/10.1039/c9ra10169a
12. Erdem H, Erdem M (2020) Synthesis and characterization of a novel activated carbon–supported cobalt catalyst from biomass mixture for tetracycline degradation via persulfate activation. Biomass Convers Biorefinery. https://doi.org/10.1007/s13399-020-00963-z
13. Evans R, Tarazona P Theory of Condensation in Narrow Capillaries
14. Fernandez J, Nadtochenko V, Kiwi J (2003) Photobleaching of Orange II within seconds using the oxone/Co2+ reagent through Fenton-like chemistry. Chem Commun 3:2382–2383. https://doi.org/10.1039/b307542g
15. Fisher P (1973) Review of Using Rhodamine B as a Marker for Wildlife Studies
16. Ghanbari F, Moradi M (2017) Application of peroxymonosulfate and its activation methods for degradation of environmental organic pollutants: Review. Chem. Eng. J. 310:41–62
17. Ghanbari F, Moradi M, Gohari F (2016) Degradation of 2,4,6-trichlorophenol in aqueous solutions using peroxymonosulfate/activated carbon/UV process via sulfate and hydroxyl radicals. J Water Process Eng 9:22–28. https://doi.org/10.1016/j.jwpe.2015.11.011

18. Ghodbane H, Hamdaoui O (2009) Intensification of sonochemical decolorization of anthraquinonic dye Acid Blue 25 using carbon tetrachloride. Ultrason Sonochem 16:455–461. https://doi.org/10.1016/j.ultsonch.2008.12.005
19. Günay T, Çimen Y (2017) Degradation of 2,4,6-trichlorophenol with peroxymonosulfate catalyzed by soluble and supported iron porphyrins. Environ Pollut 231:1013–1020. https://doi.org/10.1016/j.envpol.2017.08.059
20. Gunture, Singh A, Bhati A, et al (2019) Soluble Graphene Nanosheets for the Sunlight-Induced Photodegradation of the Mixture of Dyes and its Environmental Assessment. Sci Rep 9:. https://doi.org/10.1038/s41598-019-38717-1
21. Hardjono Y, Sun H, Tian H, et al (2011) Synthesis of Co oxide doped carbon aerogel catalyst and catalytic performance in heterogeneous oxidation of phenol in water. Chem Eng J 174:376–382. https://doi.org/10.1016/j.cej.2011.09.009
22. Hou J, He X, Zhang S, et al (2021) Recent advances in cobalt-activated sulfate radical-based advanced oxidation processes for water remediation: A review. Sci. Total Environ. 770
23. Hu L, Yang F, Lu W, et al (2013) Heterogeneous activation of oxone with CoMg/SBA-15 for the degradation of dye Rhodamine B in aqueous solution. Appl Catal B Environ 134–135:7–18. https://doi.org/10.1016/j.apcatb.2012.12.028
24. Huang YF, Huang YH (2009) Behavioral evidence of the dominant radicals and intermediates involved in Bisphenol A degradation using an efficient Co2+/PMS oxidation process. J Hazard Mater 167:418–426. https://doi.org/10.1016/j.jhazmat.2008.12.138
25. Huang YH, Huang YF, Huang C ing, Chen CY (2009) Efficient decolorization of azo dye Reactive Black B involving aromatic fragment degradation in buffered Co2+/PMS oxidative processes with a ppb level dosage of Co2+-catalyst. J Hazard Mater 170:1110–1118. https://doi.org/10.1016/j.jhazmat.2009.05.091
26. Ji Y, Shi Y, Dong W, et al (2016) Thermo-activated persulfate oxidation system for tetracycline antibiotics degradation in aqueous solution. Chem Eng J 298:225–233. https://doi.org/10.1016/j.cej.2016.04.028
27. Jiang S, Ni H, Li P, et al (2021) Metal/N-doped carbon (Metal = Ag, Cu, Ni) nanocatalysts for selective hydrogenation of 4-nitrophenol. Catal Commun 151:. https://doi.org/10.1016/j.catcom.2021.106280
28. Kamar EM, Sheha E (2017) Green synthesis of Co3O4/graphene nanocomposite as cathode for magnesium batteries. Mater Sci Pol 35:528–533. https://doi.org/10.1515/msp-2017-0076
29. Kang S, Hwang J (2021) CoMn2O4 embedded hollow activated carbon nanofibers as a novel peroxymonosulfate activator. Chem Eng J 406:. https://doi.org/10.1016/j.cej.2020.127158
30. Khan A, Zou S, Wang T, et al (2018) Facile synthesis of yolk shell Mn2O3@Mn5O8 as an effective catalyst for peroxymonosulfate activation. Phys Chem Chem Phys 20:13909–13919. https://doi.org/10.1039/c8cp02080a
31. Klepel O, Utgenannt S, Vormelchert C, et al (2021) Redox catalysts based on amorphous porous carbons. Microporous Mesoporous Mater 323:. https://doi.org/10.1016/j.micromeso.2021.111257

32. Korzeniowska A, Strzempek W, Makowski W, et al (2020) Incorporation and release of a model drug, ciprofloxacin, from non-modified SBA-15 molecular sieves with different pore sizes. Microporous Mesoporous Mater 294:. https://doi.org/10.1016/j.micromeso.2019.109903
33. Kumar A, Jena HM (2016) Preparation and characterization of high surface area activated carbon from Fox nut (Euryale ferox) shell by chemical activation with H3PO4. Results Phys 6:651–658. https://doi.org/10.1016/j.rinp.2016.09.012
34. Kwiatkowski M, Broniek E (2020) An evaluation of the reliability of the results obtained by the LBET, QSDFT, BET, and DR methods for the analysis of the porous structure of activated carbons. Materials (Basel) 13:. https://doi.org/10.3390/MA13183929
35. Le Van K, Luong Thi Thu T (2019) Preparation of pore-size controllable activated carbon from rice husk using dual activating agent and its application in supercapacitor. J Chem 2019:. https://doi.org/10.1155/2019/4329609
36. Li H, Wan J, Ma Y, et al (2016) Degradation of refractory dibutyl phthalate by peroxymonosulfate activated with novel catalysts cobalt metal-organic frameworks: Mechanism, performance, and stability. J Hazard Mater 318:154–163. https://doi.org/10.1016/j.jhazmat.2016.06.058
37. Li L, Wu H, Chen H, et al (2020a) Heterogeneous activation of peroxymonosulfate by hierarchically porous cobalt/iron bimetallic oxide nanosheets for degradation of phenol solutions. Chemosphere 256:. https://doi.org/10.1016/j.chemosphere.2020.127160
38. Li N, Lu P, He C, et al (2018) Catalytic degradation of sulfaquinoxalinum by polyester/poly-4-vinylpyridine nanofibers-supported iron phthalocyanine. Environ Sci Pollut Res 25:5902–5910. https://doi.org/10.1007/s11356-017-0943-9
39. Li Y, Ma S, Xu S, et al (2020b) Novel magnetic biochar as an activator for peroxymonosulfate to degrade bisphenol A: Emphasizing the synergistic effect between graphitized structure and CoFe2O4. Chem Eng J 387:. https://doi.org/10.1016/j.cej.2020.124094
40. Ling SK, Wang S, Peng Y (2010) Oxidative degradation of dyes in water using Co2+/H2O2 and Co2+/peroxymonosulfate. J Hazard Mater 178:385–389. https://doi.org/10.1016/j.jhazmat.2010.01.091
41. Liu C, Pan D, Tang X, et al (2016) Degradation of Rhodamine B by the α-MnO2/Peroxymonosulfate System. Water Air Soil Pollut 227:. https://doi.org/10.1007/s11270-016-2782-6
42. Lu M, Hu X, Hu Q, et al (2021) Selective oxidation of benzyl alcohol to benzaldehyde with air using ZIF-67 derived catalysts. Colloids Surfaces A Physicochem Eng Asp 629:. https://doi.org/10.1016/j.colsurfa.2021.127520
43. Mahamallik P, Pal A (2020) Photo-Fenton process in Co(II)-adsorbed admicellar soft-template on alumina support for methyl orange degradation. Catal Today 348:212–222. https://doi.org/10.1016/j.cattod.2019.07.045
44. Martínez-Huitle CA, Brillas E (2009) Decontamination of wastewaters containing synthetic organic dyes by electrochemical methods: A general review. Appl. Catal. B Environ. 87:105–145

45. Nippatla N, Philip L (2020) Electrochemical process employing scrap metal waste as electrodes for dye removal. J Environ Manage 273:. https://doi.org/10.1016/j.jenvman.2020.111039
46. Olmez-Hanci T, Arslan-Alaton I, Dursun D, et al (2015) Degradation and toxicity assessment of the nonionic surfactant Triton^{TM} X-45 by the peroxymonosulfate/UV-C process. Photochem Photobiol Sci 14:569–575. https://doi.org/10.1039/c4pp00230j
47. Pang Y, Kong L, Chen D, et al (2020) Facilely synthesized cobalt doped hydroxyapatite as hydroxyl promoted peroxymonosulfate activator for degradation of Rhodamine B. J Hazard Mater 384:. https://doi.org/10.1016/j.jhazmat.2019.121447
48. Pearce CI, Lloyd JR, Guthrie JT (2003) The removal of colour from textile wastewater using whole bacterial cells: A review. Dye. Pigment. 58:179–196
49. Pi Y, Gao H, Cao Y, et al (2020) Cobalt ferrite supported on carbon nitride matrix prepared using waste battery materials as a peroxymonosulfate activator for the degradation of levofloxacin hydrochloride. Chem Eng J 379:. https://doi.org/10.1016/j.cej.2019.122377
50. Qi F, Chu W, Xu B (2013) Catalytic degradation of caffeine in aqueous solutions by cobalt-MCM41 activation of peroxymonosulfate. Appl Catal B Environ 134–135:324–332. https://doi.org/10.1016/j.apcatb.2013.01.038
51. Rasalingam S, Wu CM, Koodali RT (2015) Modulation of pore sizes of titanium dioxide photocatalysts by a facile template free hydrothermal synthesis method: Implications for photocatalytic degradation of rhodamine B. ACS Appl Mater Interfaces 7:4368–4380. https://doi.org/10.1021/am508883f
52. Ren M, Liu H, Qu J, et al (2018) The different paths and potential risks of photo(-electro)-catalytic degradation for rhodamine B in water by graphene/TiO2 membrane. Environ Sci Pollut Res 25:13988–13999. https://doi.org/10.1007/s11356-018-1611-4
53. Roberts ALK, Fletcher JM, Moore L, Byers S (2010) Trans-generational exposure to low levels of rhodamine B does not adversely affect litter size or liver function in murine mucopolysaccharidosis type IIIA. Mol Genet Metab 101:208–213. https://doi.org/10.1016/j.ymgme.2010.06.008
54. Sanromán MA, Pazos M, Ricart MT, Cameselle C (2004) Electrochemical decolourisation of structurally different dyes. Chemosphere 57:233–239. https://doi.org/10.1016/j.chemosphere.2004.06.019
55. Song Q, Feng Y, Wang Z, et al (2019) Degradation of triphenyl phosphate (TPhP) by CoFe2O4-activated peroxymonosulfate oxidation process: Kinetics, pathways, and mechanisms. Sci Total Environ 681:331–338. https://doi.org/10.1016/j.scitotenv.2019.05.105
56. Sundar M, Easwaramoorthy D, Kutti Rani S, Mohammed Bilal I (2008) Mn(II) catalysed decomposition of peroxomonosulphate - Kinetic and mechanistic study. Catal Commun 9:2340–2344. https://doi.org/10.1016/j.catcom.2008.05.024
57. Tabit R, Amadine O, Essamlali Y, et al (2018) Magnetic CoFe2O4 nanoparticles supported on graphene oxide (CoFe2O4/GO) with high catalytic activity for peroxymonosulfate activation and degradation of rhodamine B. RSC Adv 8:1351–1360. https://doi.org/10.1039/c7ra09949e

58. TUINSTRA F, KOENIG JL (1970) RAMAN SPECTRUM OF GRAPHITE. J Chem Phys 53:1126–1130. https://doi.org/10.1063/1.1674108
59. Üner O, Bayrak Y (2018) The effect of carbonization temperature, carbonization time and impregnation ratio on the properties of activated carbon produced from Arundo donax. Microporous Mesoporous Mater 268:225–234. https://doi.org/10.1016/j.micromeso.2018.04.037
60. Upadhyay GK, Rajput JK, Pathak TK, et al (2020) Photoactive CdO:TiO2 nanocomposites for dyes degradation under visible light. Mater Chem Phys 253:. https://doi.org/10.1016/j.matchemphys.2020.123191
61. Valdés H, Sánchez-Polo M, Rivera-Utrilla J, Zaror CA (2002) Effect of ozone treatment on surface properties of activated carbon. Langmuir 18:2111–2116. https://doi.org/10.1021/la010920a
62. Wan Z, Wang J (2017) Fenton-like degradation of sulfamethazine using Fe3O4/Mn3O4 nanocomposite catalyst: kinetics and catalytic mechanism. Environ Sci Pollut Res 24:568–577. https://doi.org/10.1007/s11356-016-7768-9
63. Wang W, Yao H, Yue L (2020a) Supported-catalyst CuO/AC with reduced cost and enhanced activity for the degradation of heavy oil refinery wastewater by catalytic ozonation process. Environ Sci Pollut Res 27:7199–7210. https://doi.org/10.1007/s11356-019-07410-1
64. Wang X, Deng B, Yu L, et al (2020b) Degradation of azo dyes Congo red by MnBi alloy powders: Performance, kinetics and mechanism. Mater Chem Phys 251:. https://doi.org/10.1016/j.matchemphys.2020.123096
65. Wang Y, Cao J, Yang Z, et al (2021) Fabricating iron-cobalt layered double hydroxide derived from metal-organic framework for the activation of peroxymonosulfate towards tetracycline degradation. J Solid State Chem 294:121857. https://doi.org/10.1016/j.jssc.2020.121857
66. Wang YR, Chu W (2011) Degradation of a xanthene dye by Fe(II)-mediated activation of Oxone process. J Hazard Mater 186:1455–1461. https://doi.org/10.1016/j.jhazmat.2010.12.033
67. Xiao J, Xie Y, Rabeah J, et al (2020) Visible-Light Photocatalytic Ozonation Using Graphitic C3N4 Catalysts: A Hydroxyl Radical Manufacturer for Wastewater Treatment. Acc Chem Res 53:1024–1033. https://doi.org/10.1021/acs.accounts.9b00624
68. Xie H (2017) Activation of persulfate by MMIOC for highly efficient degradation of rhodamine B. RSC Adv 7:45624–45633. https://doi.org/10.1039/c7ra07645b
69. Xu M, Li J, Yan Y, et al (2019) Catalytic degradation of sulfamethoxazole through peroxymonosulfate activated with expanded graphite loaded CoFe2O4 particles. Chem Eng J 369:403–413. https://doi.org/10.1016/j.cej.2019.03.075
70. Yang Q, Choi H, Chen Y, Dionysiou DD (2008) Heterogeneous activation of peroxymonosulfate by supported cobalt catalysts for the degradation of 2,4-dichlorophenol in water: The effect of support, cobalt precursor, and UV radiation. Appl Catal B Environ 77:300–307. https://doi.org/10.1016/j.apcatb.2007.07.020
71. Yang Y, Jiang J, Lu X, et al (2015) Production of Sulfate Radical and Hydroxyl Radical by Reaction of Ozone with Peroxymonosulfate: A Novel Advanced Oxidation Process. Environ Sci Technol

49:73307339. https://doi.org/10.1021/es506362e

72. Yazdanbakhsh A, Aliyari A, Sheikhmohammadi A, Aghayani E (2020) Application of the enhanced sono-photo-Fenton-like process in the presence of persulfate for the simultaneous removal of chromium and phenol from the aqueous solution. J Water Process Eng 34:. https://doi.org/10.1016/j.jwpe.2019.101080
73. Yuan R, Ramjaun SN, Wang Z, Liu J (2011) Effects of chloride ion on degradation of Acid Orange 7 by sulfate radical-based advanced oxidation process: Implications for formation of chlorinated aromatic compounds. J Hazard Mater 196:173–179. https://doi.org/10.1016/j.jhazmat.2011.09.007
74. Yuan X, Zheng W, Feng S, et al (2021) Degradation of bisphenol A through Ti–BiOI/ZIF-8/peroxymonosulfate (PMS): Catalyst preparation, experimental design and catalytic mechanism. J Solid State Chem 304:122596. https://doi.org/10.1016/j.jssc.2021.122596
75. Zhang D, Li Y, Guo J, et al (2021) MOFs-derived magnetic C@Cu–Ni bimetal particles: An efficient peroxymonosulfate activator for 2,4,6-trichlorophenol degradation. Chemosphere 269:. https://doi.org/10.1016/j.chemosphere.2020.129394
76. Zhang H, Li C, Lyu L, Hu C (2020) Surface oxygen vacancy inducing peroxymonosulfate activation through electron donation of pollutants over cobalt-zinc ferrite for water purification. Appl Catal B Environ 270:. https://doi.org/10.1016/j.apcatb.2020.118874
77. Zhao L, Yang D, Ma L, et al (2021) An efficient heterogeneous catalyst of FeCo2O4/g-C3N4 composite for catalytic peroxymonosulfate oxidation of organic pollutants under visible light. Colloids Surfaces A Physicochem Eng Asp 610:. https://doi.org/10.1016/j.colsurfa.2020.125725
78. Zhu J, Zhu Z, Zhang H, et al (2019) Calcined CoAl-layered double hydroxide as a heterogeneous catalyst for the degradation of acetaminophen and rhodamine B: activity, stability, and mechanism. Environ Sci Pollut Res 26:33329–33340. https://doi.org/10.1007/s11356-019-06390-6
79. Zuo S, Xia D, Guan Z, et al (2021) Magnetite/graphite carbon nitride composite for peroxymonosulfate non-radical activation. Colloids Surfaces A Physicochem Eng Asp 611:. https://doi.org/10.1016/j.colsurfa.2020.125895

Figures

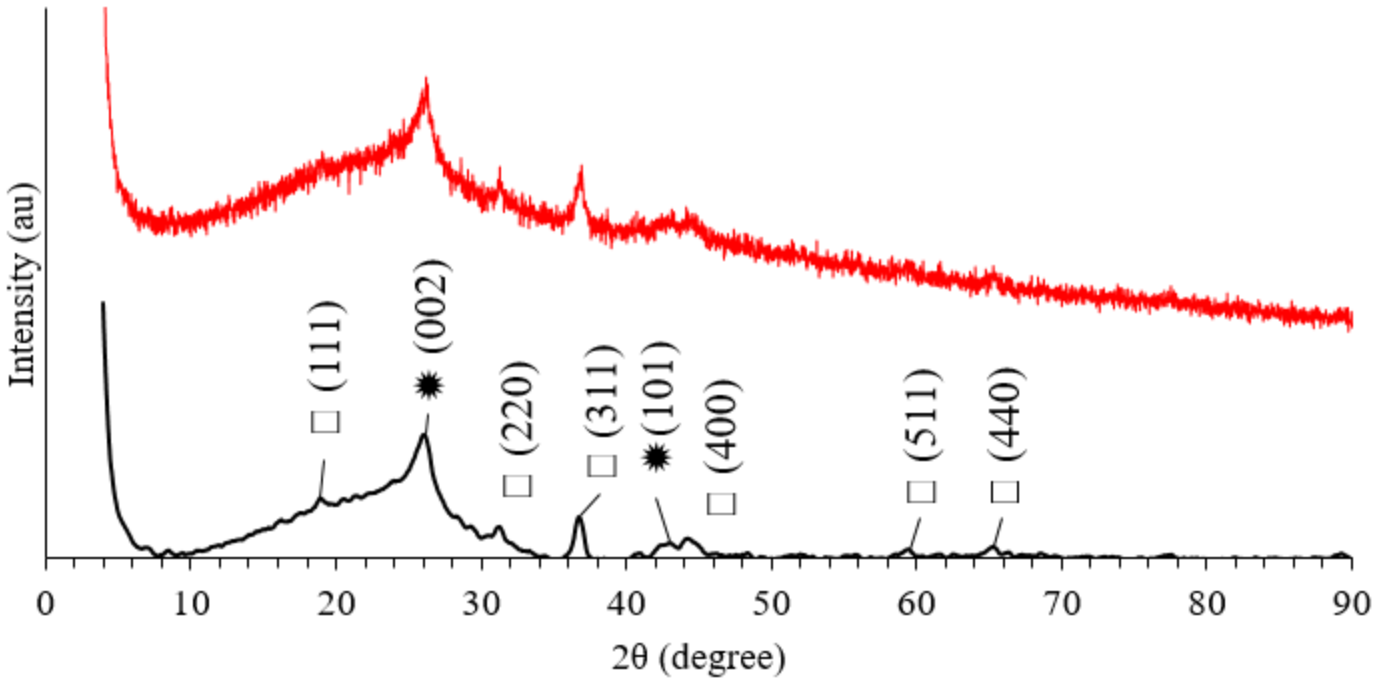

Figure 1

a) XRD pattern of Co-AC, b) Normalized and smoothed XRD pattern of Co-AC (£: Co3O4 and ð: carbon peaks)

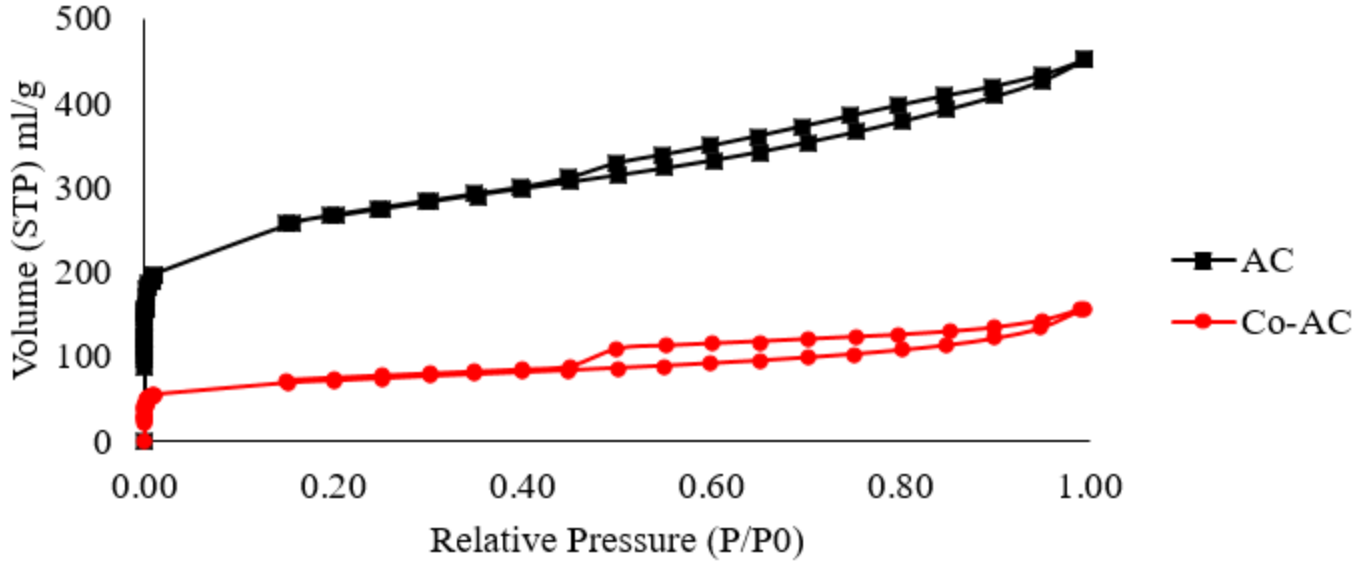

Figure 2

Adsorption and desorption isotherms of AC and Co-AC

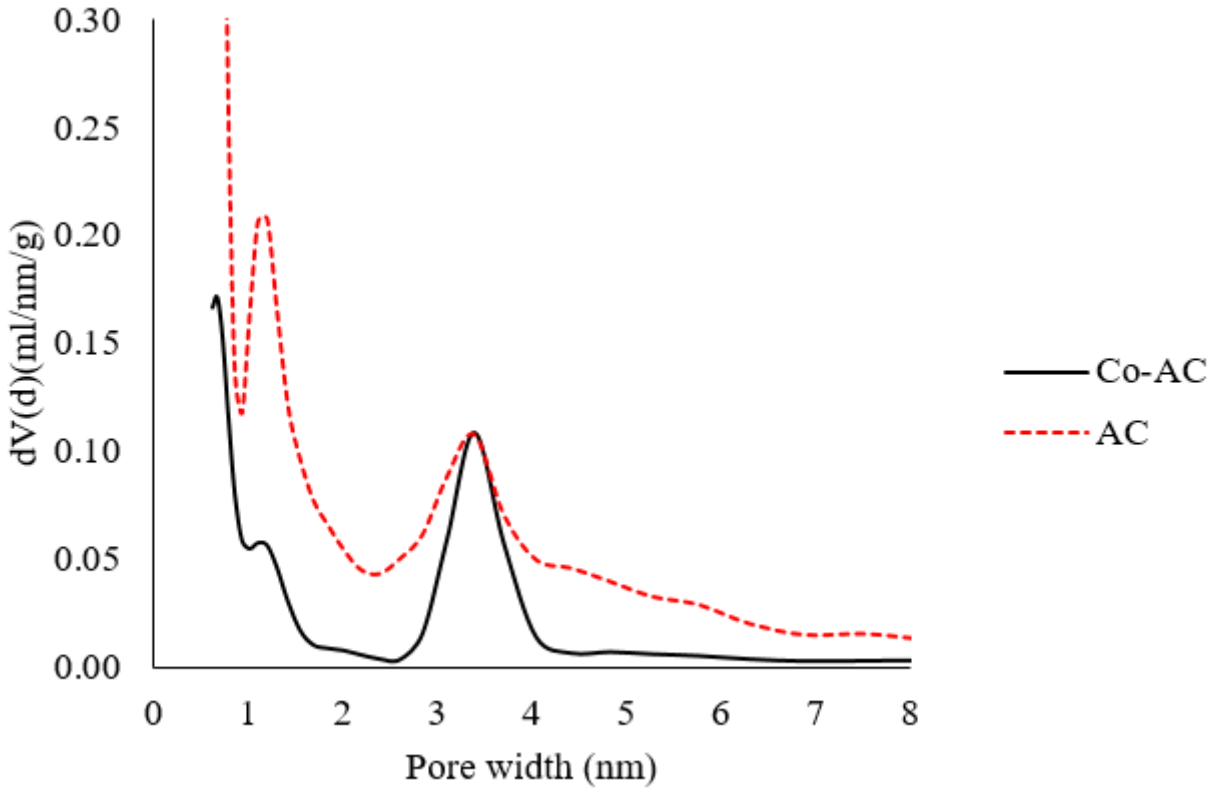

Figure 3

Pore size distribution of AC and Co-AC determined by QS-DFT method

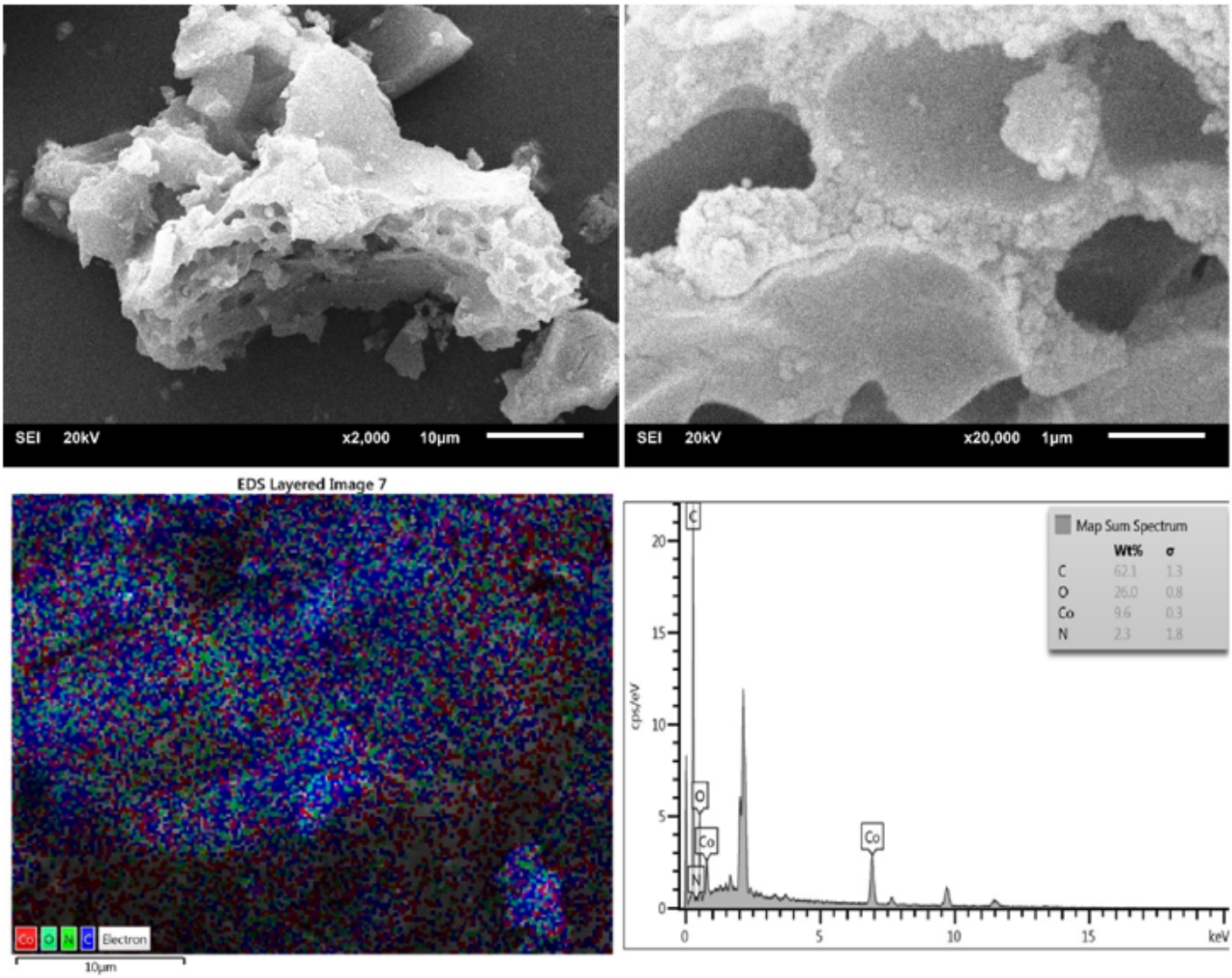

Figure 4

SEM images, EDS map and elemental distribution of Co-AC

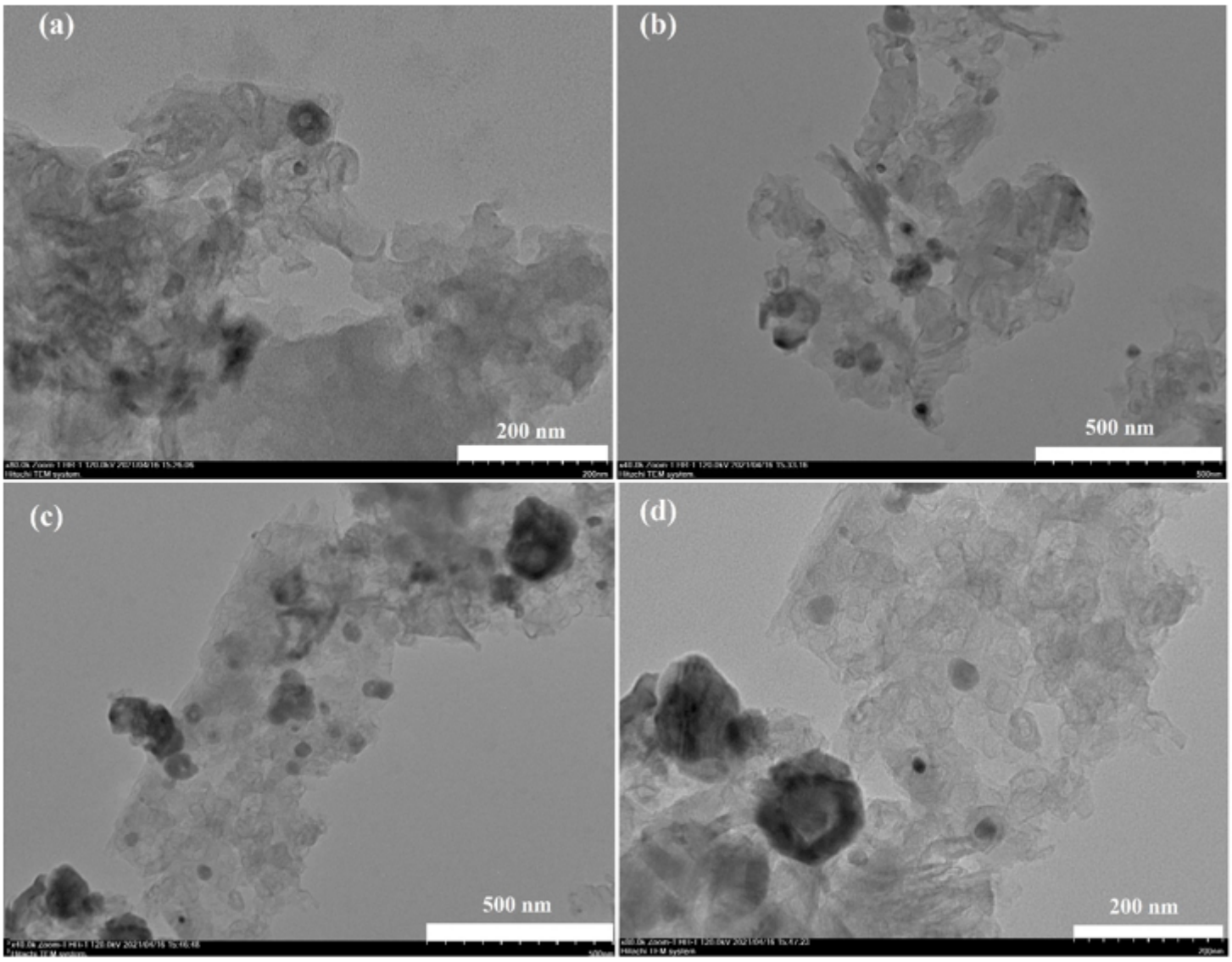

Figure 5

TEM images of Co-AC

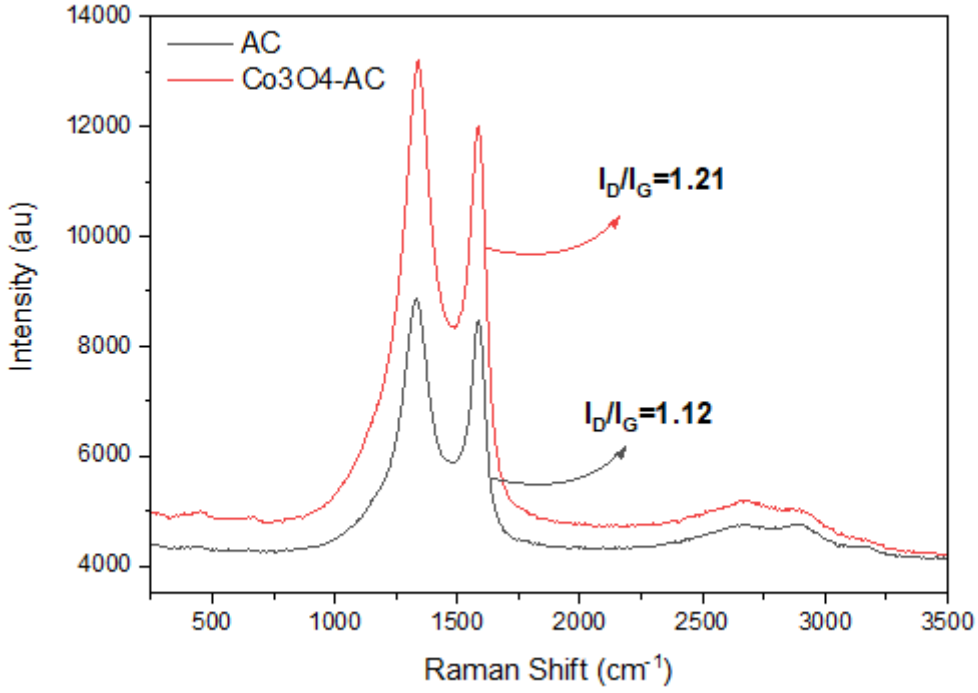

Figure 6

Raman spectra of AC and Co-AC

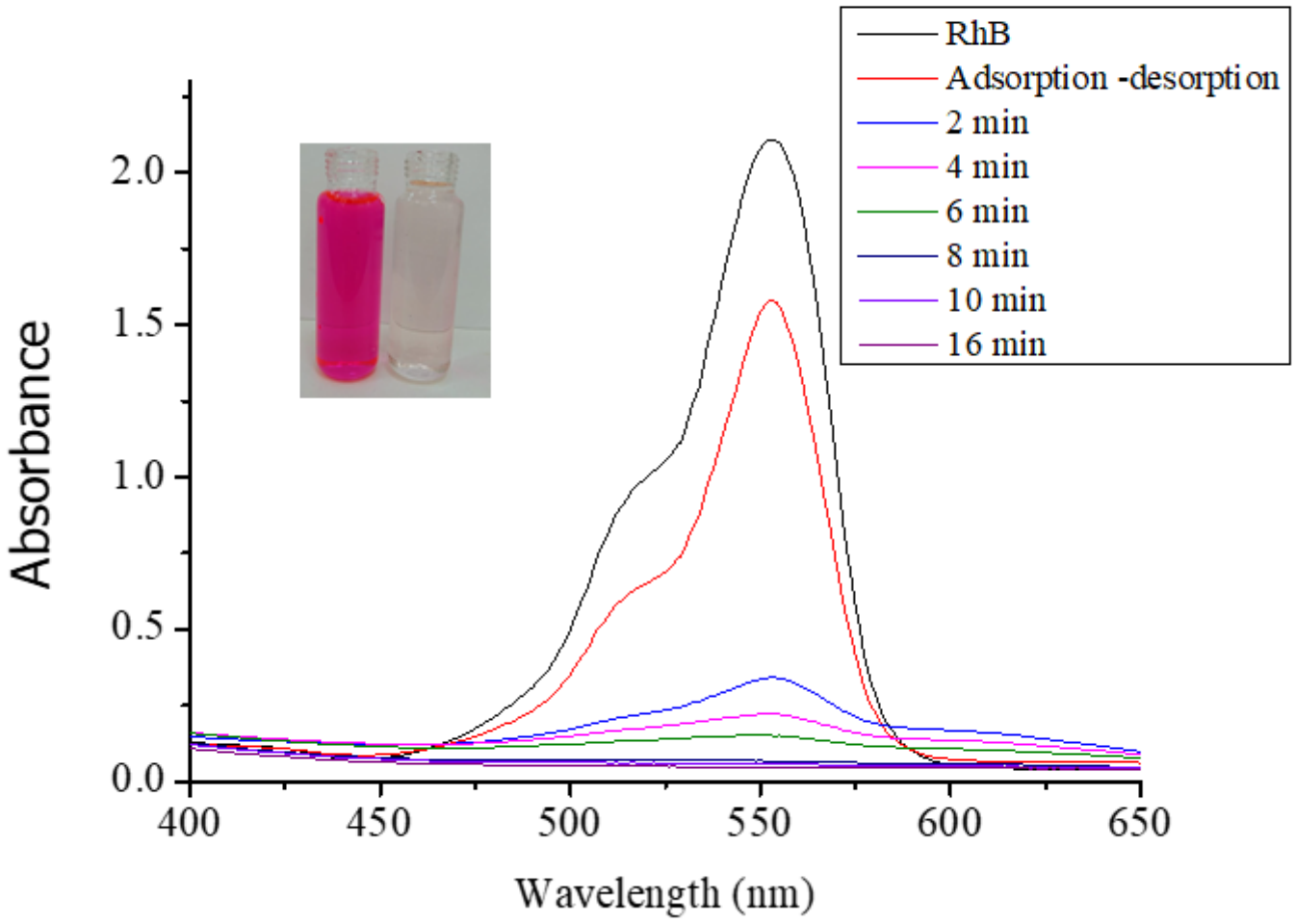

Figure 7

UV-vis absorption spectra of RhB degradation. Reaction conditions: [RhB]= 12 mgL^{-1}, [Catalyst]= 150 mgL^{-1}, [PMS]= 90 mgL^{-1}, temperature = 25 ^{o}C.

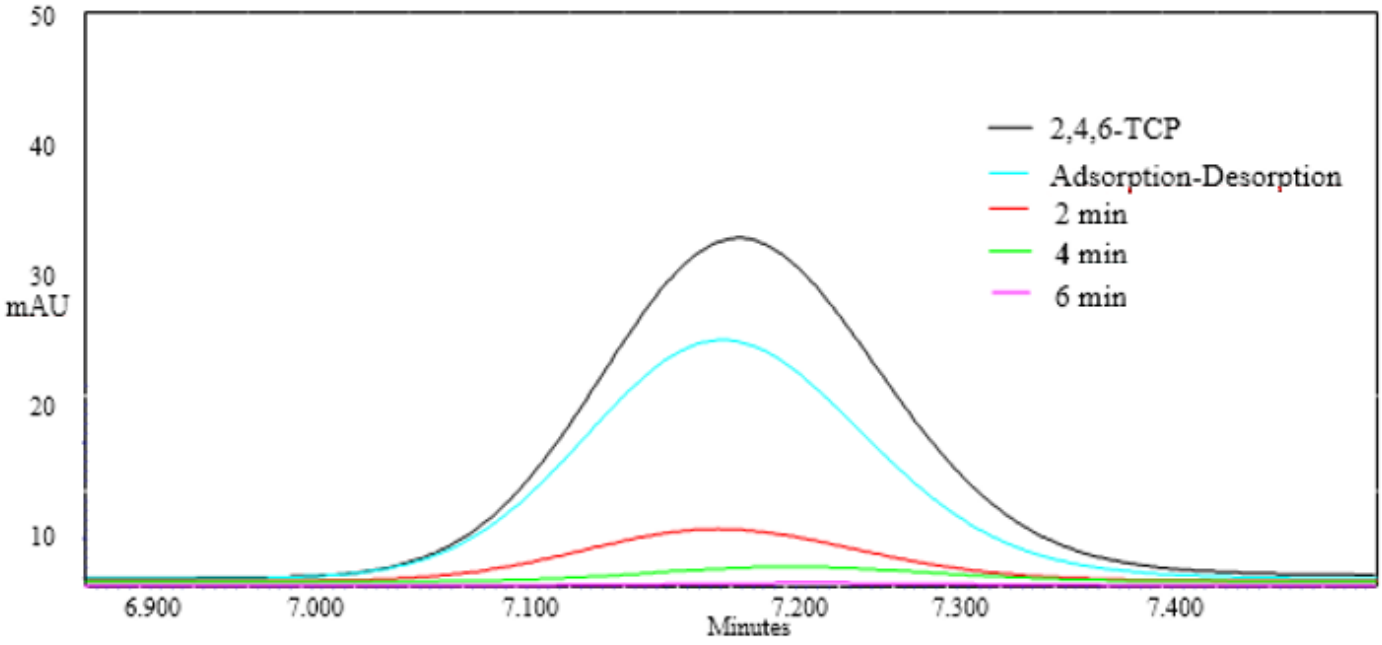

Figure 8

Absorption spectra of 2,4,6-TCP degradation. [2,4,6-TCP]= 25 mgL^{-1}, [Catalyst]= 150 mgL^{-1}, [PMS]= 90 mgL^{-1}, temperature = 25 ^{o}C.

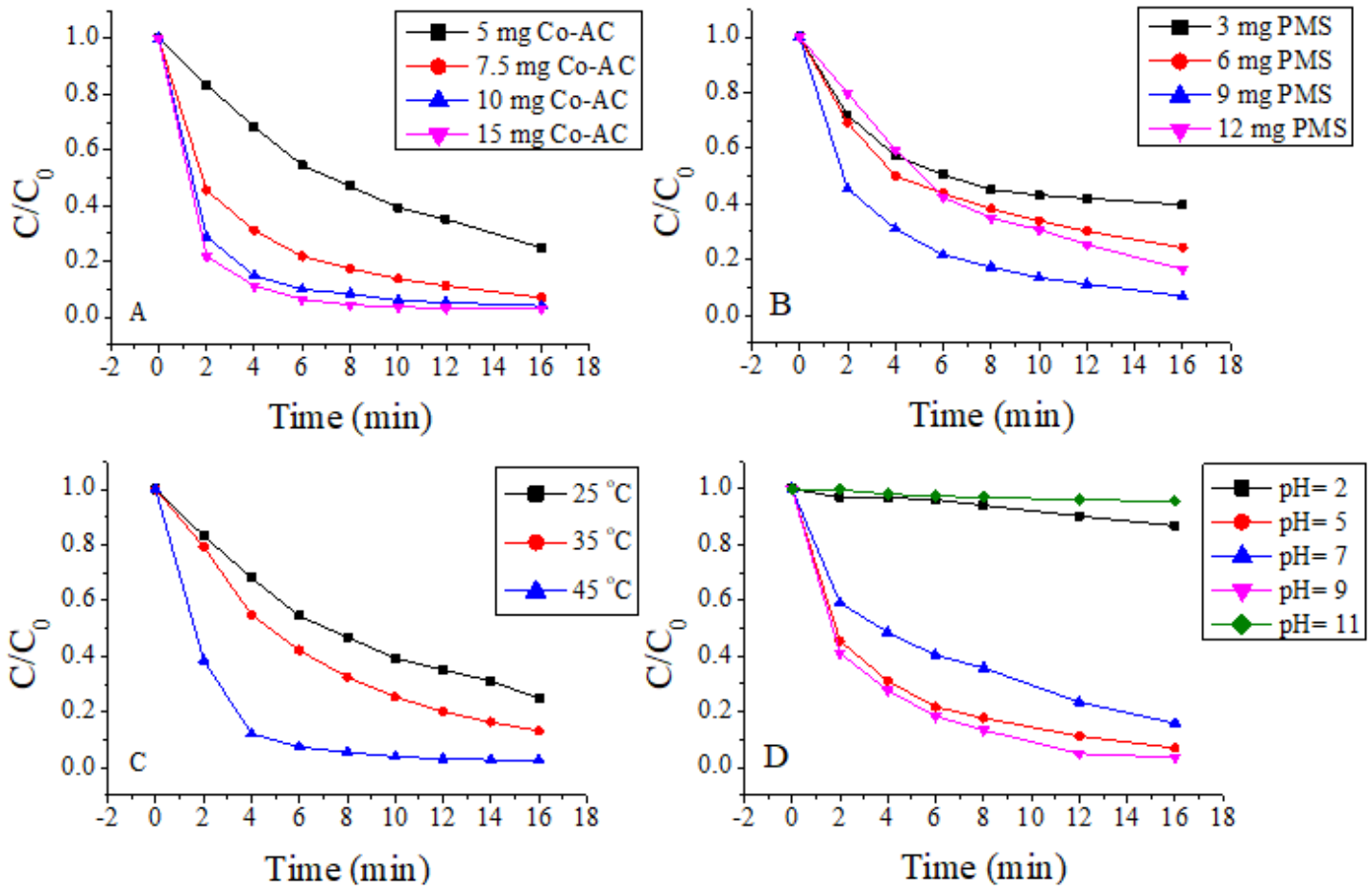

Figure 9

(A) Effect of catalyst concentration on RhB degradation. Reaction conditions: [RhB]= 12 mgL^{-1}, [PMS]= 90 mgL^{-1}, temperature = 25 ^{o}C. (B) Effect of PMS concentration on RhB degradation. Reaction conditions: [RhB]= 12 mgL^{-1}, [Catalyst]= 75 mgL^{-1}, temperature = 25 ^{o}C. (C) Effect of temperature on RhB degradation. Reaction conditions: [RhB]= 12 mgL^{-1}, [Catalyst]= 50 mgL^{-1}, [PMS]= 90 mg/L. (D) Effect of pH on RhB degradation. Reaction conditions: [RhB]= 12 mgL^{-1}, [PMS]= 90 mgL^{-1}, [Catalyst]= 75 mgL^{-1}, temperature = 25 ^{o}C.

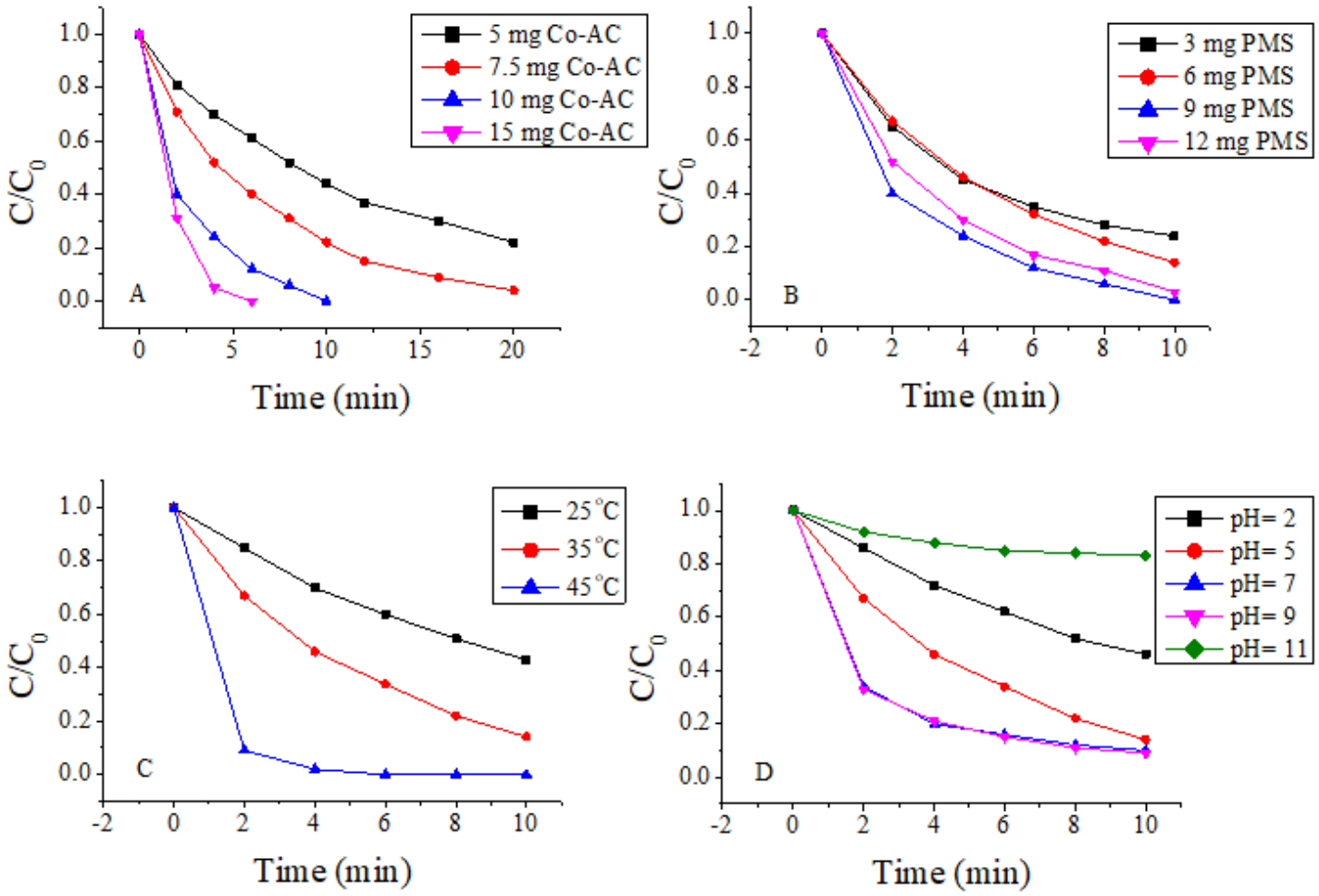

Figure 10

(A) Effect of catalyst concentration on 2,4,6-TCP degradation. Reaction conditions: [2,4,6-TCP]= 25 mgL^{-1}, [PMS]= 90 mgL^{-1}, temperature = 25 ^{o}C. (B) Effect of PMS concentration on 2,4,6-TCP degradation. Reaction conditions: [2,4,6-TCP]= 25 mgL^{-1}, [Catalyst]= 100 mgL^{-1}, temperature = 25 ^{o}C. (C) Effect of temperature on 2,4,6-TCP degradation. Reaction conditions: [2,4,6-TCP]= 25 mgL^{-1}, [Catalyst]= 100 mgL^{-1}, [PMS]= 60 mgL^{-1}. (D) Effect of pH on 2,4,6-TCP degradation. Reaction conditions: [2,4,6-TCP]= 25 mgL^{-1}, [Catalyst]= 100 mgL^{-1}, [PMS]= 60 mgL^{-1}, temperature = 25 ^{o}C.

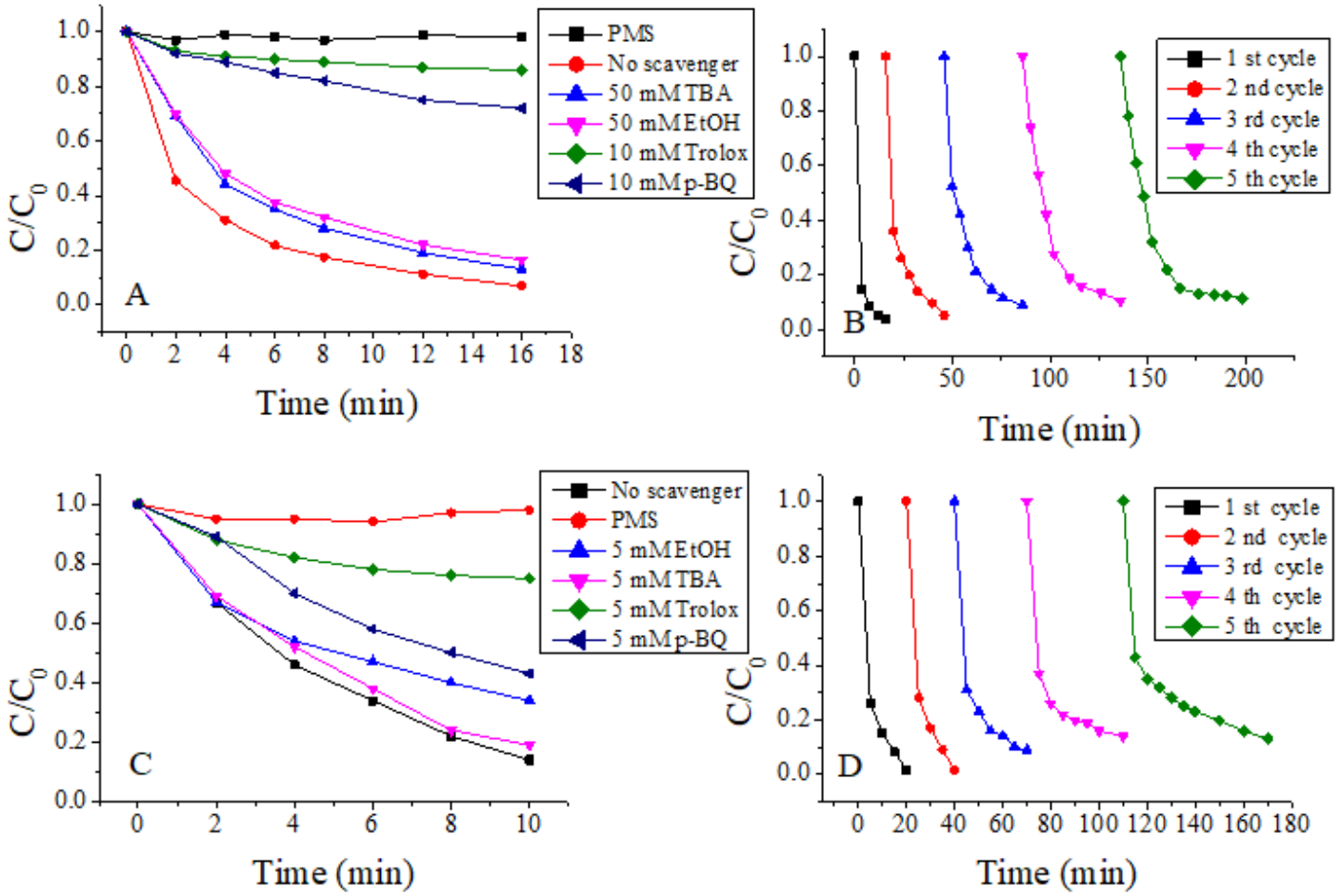

Figure 11

(A) Radical quenching experiments of RhB. Reaction conditions: [RhB]= 12 mgL^{-1}, [Catalyst]= 75 mgL^{-1}, [PMS]= 90 mgL^{-1}, temperature = 25 ^{o}C. (B) Experiment of reusability of catalyst on RhB degradation. Reaction conditions: [RhB]= 12 mgL^{-1}, [Catalyst]= 100 mgL^{-1}, [PMS]= 90 mgL^{-1}, temperature = 25 ^{o}C. (C) Radical quenching experiments of 2,4,6-TCP degradation. Reaction conditions: [2,4,6-TCP]= 25 mgL^{-1}, [Catalyst]= 100 mgL^{-1}, [PMS]= 60 mgL^{-1}, temperature = 25 ^{o}C. (D) Experiment of reusability of catalyst on 2,4,6-TCP degradation. Reaction conditions: [2,4,6-TCP]= 25 mgL^{-1}, [Catalyst]= 100 mgL^{-1}, [PMS]= 60 mgL^{-1}, temperature = 25 ^{o}C.

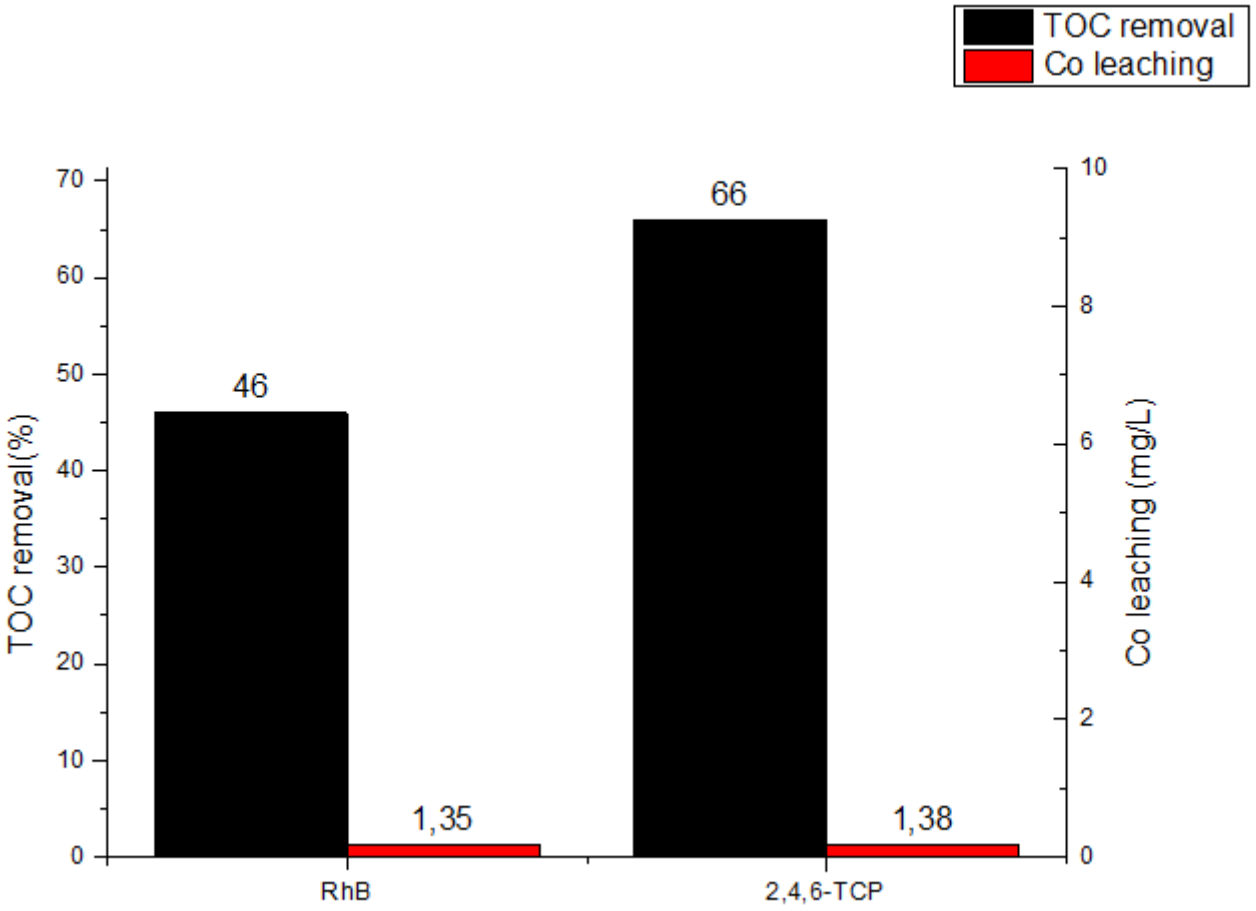

Figure 12

TOC and Co leaching values of RhB and 2,4,6- TCP at the end of reaction. (Reaction conditions for TOC and ICP-OES analysis: [Catalyst]= 100 mgL^{-1}, [RhB]= 12 mgL^{-1}, [PMS]= 60 mgL^{-1} and temperature= 25 ^{o}C for RhB/Co-AC system and [Catalyst]= 100 mgL^{-1}, [2,4,6-TCP]= 25 mgL^{-1}, [PMS]= 90 mgL^{-1} and temperature= 25 ^{o}C for 2,4,6-TCP /Co-AC system also no pH adjustiment for RhB and 2,4,6-TCP).